INL/RPT-24-80381
Revision 0

Light Water Reactor Sustainability Program

Virtual Demonstration of Flexible Hydrogen Production Using Nuclear Power as Non-Spinning Reserve Capacity Supporting High Penetration of Wind and Solar Power

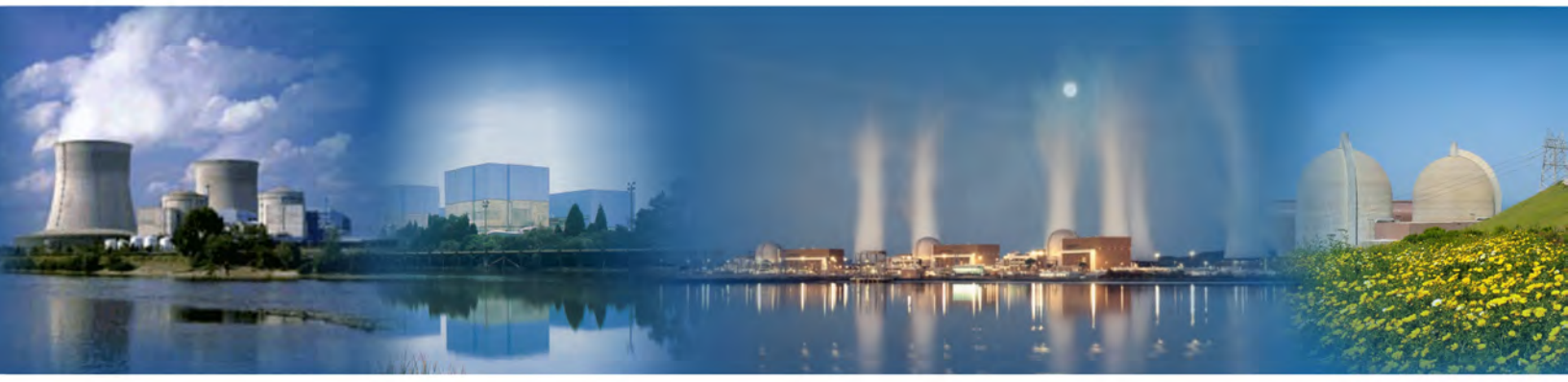

August 2024
U.S. Department of Energy
Office of Nuclear Energy

INL/RPT-24-80381
Revision 0

Virtual Demonstration of Flexible Hydrogen Production Using Nuclear Power as Non-Spinning Reserve Capacity Supporting High Penetration of Wind and Solar Power

Bikash Poudel, Temitayo O. Olowu, Jianqiao Huang, Tyler L. Westover

August 2024

Prepared for the
U.S. Department of Energy
Office of Nuclear Energy

EXECUTIVE SUMMARY

This Light Water Reactor Sustainability (LWRS) program with the Department of Energy (DOE) has established a pathway to research flexible power operations for existing U.S. nuclear reactors to improve plant economics while accommodating increasing penetration of variable renewable wind and solar generation on the bulk power grid. The Flexible Plant Operation and Generation (FPOG) pathway within LWRS has coordinated several research efforts to assess nuclear power plant (NPP) modifications that enable the use of large-scale thermal energy (steam) and electricity to support the production of alternative clean energy products, which can compete economically with current nuclear operations. Hydrogen is recognized as a leading clean energy product because it is a critical feedstock for a variety of products, including fuels, chemicals, and fertilizers, as well as an important component in decarbonizing hard-to-abate sectors, such as heavy industry, long-haul transport, and energy storage. Currently, hydrogen production is carbon-intensive; however, clean hydrogen can be produced via electrolysis when powered by renewable or nuclear energy sources. Due to its high efficiency and potentially low hydrogen production cost, this report specifically focuses on hydrogen production via high-temperature steam electrolysis (HTSE) plants that are coupled to NPPs as a source of electrical and thermal energy.

This report describes simulations that were performed to analyze the coupled performance of integrated energy systems that include nuclear power and solid oxide electrolysis cell (SOEC) hydrogen production in a power grid environment. For the simulations, a 4-loop pressurized water reactor (PWR) plant and an SOEC plant were modeled in Matlab/Simulink and connected to a modified IEEE 39-bus transmission grid network modeled in RSCAD. The system consists of 10 generators, several bus loads, transmission lines and capacitor banks.

Several scenarios were modeled to optimize potential benefits of coupled nuclear electrical and thermal power for hydrogen production while benefiting from potential ancillary market opportunities. Specifically, opportunities for participating in reserve and regulation markets in the Pennsylvania/New Jersy/Maryland (PJM) market were also explored, as well as reserve markets in California (CAISO). For a system connected to the PJM market, optimization results show that participating in both reserve and regulation markets increases revenues by 7.5%, while still adhering to contracted daily hydrogen production constraints. Real-time simulations show that the provision of ancillary services by the nuclear power plant has no adverse stability impact on the overall system and could potentially be used to improve overall system stability.

In addition to showing that LWRs can successfully operate in flexible modes to produce hydrogen, with the potential to enhance grid resilience by offering reserve capacities, this work also highlights challenges related to non-linear flow dynamics, the need for precise control systems, and the importance of integrating feedback loops to maintain thermal system performance during transitions in power output.

This work demonstrates that LWRs can play a transformative role in the clean energy transition by diversifying their operational capabilities and contributing to hydrogen production, ensuring reliable power supply while supporting decarbonization efforts. These findings provide valuable insights for stakeholders considering the deployment of LWRs for dual-purpose energy and hydrogen production. Furthermore, integrating these simulators with grid power resources is a key step toward using pilot-scale SOEC systems with a simulated PWR and power grid environment to verify concepts of integrated nuclear/hydrogen production operations.

CONTENTS

FIGURES

TABLES

ACRONYMS

BoP	balance of plant
CAISO	California Independent System Operator
DSL	delivery steam line
FPOG	flexible plant operations and generation
FWH	feedwater heater
GHG	greenhouse gas
HIL	hardware-in-the-loop
HP	high pressure
HPFWH	high pressure feedwater heater
HPT	high pressure turbine
HTSE	high-temperature electrolysis
IEEE	Institute of Electrical and Electronics Engineers
INL	Idaho National Laboratory
LMP	locational marginal pricing
LP	low pressure
LPFWH	low pressure feedwater heater
LPT	low pressure turbine
LTWE	low-temperature water electrolysis
LWR	light water reactor
NPP	nuclear power plant
PJM	Pennsylvania-New Jersey-Maryland
POI	point of interconnection
PR	primary reserve
PV	photovoltaic
PWR	pressurized water reactor
RO	reduced order
RPV	reactor pressure vessel
RSCAD	Real-Time Simulator for Computer-Aided Design
RTDS	real-time digital simulator
RTO	Regional Transmission Organization
RD	regulation down
RU	regulation up
S&L	Sargent and Lundy

SOEC	solid oxide electrolyzer cell
SR	synchronous reserve
TPD	thermal power dispatch
XSL	extraction steam line

Virtual Demonstration of Flexible Hydrogen Production Using Nuclear Power as Non-Spinning Reserve Capacity Supporting High Penetration of Wind and Solar Power

1. INTRODUCTION

To meet the global decarbonization mandate, an equitable and sustainable clean energy transition is necessary across the entire spectrum of energy usage. Energy use represents roughly three-quarters of global greenhouse gas emissions, mainly originating from the use of heat and electricity in buildings, transport, and industries [1]. In recent years, global investment in clean energy has significantly outpaced spending on fossil fuels, which clearly indicates the world's commitment to decarbonization [2]. The U.S. in particular aims to reduce GHG emissions 50% below 2005 levels by 2030 and achieve economy-wide net-zero emissions by no later than 2050. Multiple pathways have been identified, ranging from decarbonizing electricity, reducing energy waste, switching to clean fuels, capturing and removing carbon from the atmosphere, and reducing other non-CO_2 GHG emissions [3]. Although solutions are identified in each sector, there are significant challenges, particularly in the hard-to-abate heavy industry and long-distance transport sectors. Similarly, there are concerns about over-reliance on uncertain and intermittent renewable energy resources to meet decarbonization mandates.

Hydrogen is widely recognized as a necessary tool to deliver economy-wide decarbonization options for various hard-to-abate sectors, including long-haul transport, chemical production, iron and steel manufacturing, and long-duration energy storage, in addition to its current use in ammonia production. Currently, hydrogen is predominantly produced through the steam methane reforming process, which releases 8-10 kg CO_2 per kilogram of hydrogen product. However, clean hydrogen can be produced via electrolysis when powered with energy (electrons and heat) from clean energy resources.

Electrolytic hydrogen production can be broadly categorized into two types: low-temperature water electrolysis (LTE) and high-temperature steam electrolysis (HTSE). While LTE technologies split water into hydrogen and oxygen at lower temperatures (60-80°C) using electricity only, HTSE technologies split steam at high temperatures (650-850°C) using both heat and electricity. Electricity can be provided by any clean electric generation technology. The heat can be provided by electric heaters, heat pumps, or directly from nuclear or other thermal power plants. HTSE, due to its lower net energy requirements for electrolysis at higher temperatures, offers superior efficiency despite being less flexible to control than LTE in the near-term. The prospect of electrolytic hydrogen production through a variety of clean generation technologies, such as wind, solar, hydropower, marine, and conventional and advanced nuclear power resources is being investigated.

Some light water reactor (LWR) facilities in the United States are evaluating options for transitioning from baseload electricity production to directly providing clean power to electrolysis hydrogen production facilities. However, the loss of large-scale nuclear plants on the power grid, with their firm power and mechanical inertia, would increase grid vulnerability, particularly for areas that have a large share of intermittent renewable energy generation. The Light Water Reactor Sustainability (LWRS) Program of the Department of Energy (DOE) is assisting utilities in nuclear power plant modernization efforts to enable nuclear plants to continue providing power resources to the grid through more cost-efficient power production as well as developing flexible plant operating strategies, including diversification of revenue streams.

Provided that the existing and new market incentives are attractive enough, flexible LWR hydrogen production presents benefits for both the grid and the nuclear power plant. To this end, this report aims to (1) develop a comprehensive production optimization model of flexible LWR hydrogen production considering both power and ancillary market revenue streams, and (2) develop real-time operation simulation models to understand the system stability and dynamics for operating flexible LWR hydrogen

production in multiple electricity markets. This work develops the capability to understand the opportunities and challenges of grid-connected flexible LWR hydrogen production to provide guidelines for these operations.

2. SYSTEM MODELS

The models used in this analysis includes pressurized water reactor (PWR)-based NPP with flexible thermal dispatch based on the 4-loop PWR design by Sargent and Lundy (S&L), and solid oxide electrolyzer cell (SOEC)-based high temperature electrolysis process. We map the control characteristics of LWR coupled to hydrogen production to evaluate grid power and ancillary market opportunities.

2.1 Nuclear Power Plant Model with TPD

Three nuclear power plant models are introduced in this work. The first is a quasi-steady state, reduced-order 3-loop PWR simulator that has been modified for thermal power dispatch (TPD) that was developed using Python [4]. The second model is a similar reduced-order simulator developed in Matlab/Simulink with enhanced capabilities for performing dynamic coupled electrical and thermal power dispatch simulations [5]. The third model is a high-fidelity, steady-state 4-loop PWR model developed in PEPSE (Performance Evaluation of Power System Efficiencies from Curtiss-Wright) by Sargent & Lundy (S&L) that also includes integrated thermal power dispatch (TPD) [6].

The process flow diagram of the reduced-order Matlab/Simulink 4-loop PWR-TPD simulator is depicted in Figure 1. Key design features of the simulator include:

- Two reheaters between high- and low-pressure turbines. A portion of first stage extraction from high-pressure turbine is used as heating fluid in first-stage reheater, whereas the second stage reheater uses a portion of main steam.
- The moisture separator feeds directly into a heater drain tank and is then sent to a single high-pressure feedwater heater (HPFWH).
- A single low-pressure feedwater heater (LPFWH) accepts extraction steam from the low-pressure turbine.

Sargent & Lundy performed steady-state system analyses for dispatching 0%, 30%, 50%, and 70% of the rated reactor power using their PEPSE model [6], and these results provided the benchmark data for the other models. We observed that although the heat input and process supply steam remain at nominal conditions, the extraction flows and pressures exhibit a nonlinear trend across different TPD levels. This suggests that the control setpoints were adjusted to optimize operational performance at lower TPD extraction levels. Additionally, turbine efficiency varies inconsistently across different TPD extraction levels. Apart from these design differences, the system's physical parameters and thermodynamic state variables also change with varying power and extraction levels. This information is available in [6].

Table 1 presents pressure, extraction flow, and enthalpy at selected nodes of the secondary coolant circuit for different TPD extraction levels, based on the Matlab/Simulink 4-loop PWR-TPD simulator. These selected nodes serve as control points for the secondary coolant circuit. The variables at these nodes are set as control targets in both reduced-order models.

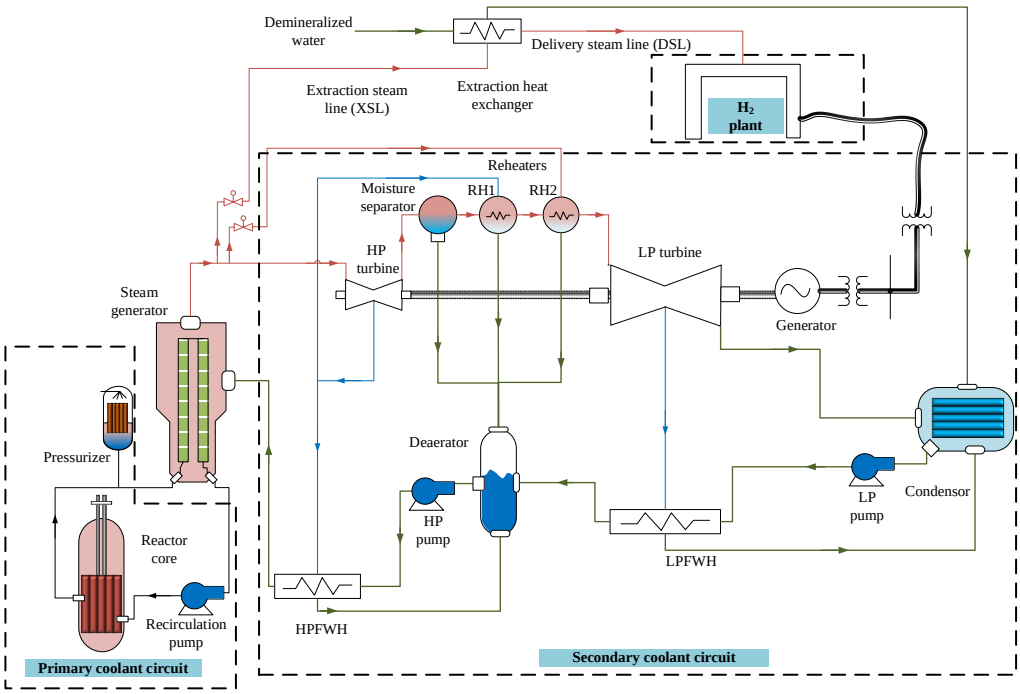

Figure 1. Reduced-order PWR-TPD with a coupled high temperature steam electrolysis plant for producing hydrogen.

Table 1. Thermodynamic states at various nodes across the secondary coolant circuit for the Simulink PWR-TPD simulator

Node	Variable	TPD%			
		0%	30%	50%	70%
	Thermal Power Input (MWt)	3646.88	3646.88	3646.88	3646.88
Main Steam	Pressure (MPa)	6.19	6.19	6.19	6.19
	Enthalpy (kJ/kg)	2784.92	2784.92	2784.92	2784.92
Reheater 2 Extraction	Flow (kg/s)	99.31	93.09	87.20	79.58
HPT Extraction	Pressure (MPa)	3.01	2.11	1.50	0.90
	Flow FWH (kg/s)	329.20	249.00	182.51	103.83
	Flow RH1 (kg/s)	87.82	47.87	26.87	10.96
HPT Outlet	Pressure (MPa)	1.318	0.923	0.659	0.395
LPT Extraction	Pressure (MPa)	0.23	0.16	0.11	0.06
	Flow FWH (kg/s)	310.66	283.36	254.86	206.58
LPT Outlet	Pressure (MPa)	0.01	0.008	0.006	0.005

2.1.1 Non-Linear Python Reduced-Order PWR-TPD Simulator

Details of the Python, quasi-steady state, reduced-order (RO) PWR-TPD simulator that have been published in [4]. While the quasi-steady state Python RO model can perform steady-state mass and energy balance calculations, it cannot simulate component-specific characteristics, such as flow resistances, heat exchanger effectiveness, or predict the thermodynamic states of turbine stages during off-nominal operation. Therefore, flow and pressure ratios for different TPD levels are directly applied using a lookup table.

The Python RO PWR-TPD simulator is initialized using the initialization sequence described in [4]. By utilizing the flow and pressure ratios and the target thermal power input from the reactor's primary to secondary side, the thermodynamic state variables for the secondary coolant circuit are determined for a given TPD level. Table 2 provides the steady-state results for 0%TPD using the Python RO PWR-TPD simulator.

Table 2. Steady-state thermodynamic results for the secondary system with %TPD = 0 for the Python RO PWR-TPD simulator. *T*: temperature; *p*: pressure; *h*: enthalpy;, *s*: entropy; x: steam fraction; and ṁ: mass flow rate.

Name	T (ºC)	p (MPa)	h (kJ/kg)	*s* (kJ/kg·°C)	x	ṁ (kg/s)
bv	277.59	6.19	2782.49	5.88	1.00	0.00
gv	277.59	6.19	2782.49	5.88	1.00	2003.99
ms_reheater	277.59	6.19	2782.49	5.88	1.00	100.20
hpt_in	270.27	5.53	2782.49	5.92	1.00	1903.79
hpt_stg1	234.04	3.01	2685.39	5.95	0.93	315.52
hpt_stg1_RH	234.04	3.01	2685.39	5.95	0.93	84.18
hpt_out	192.24	1.32	2560.88	6.00	0.89	1504.09
ms_deaerator	192.25	1.32	817.57	2.26	0.00	172.66
reheater1	192.24	1.32	2786.94	6.49	1.00	1331.44
reheater2	233.69	1.32	2892.92	6.71	1.00	1331.44
reheater_1_deaerator	234.02	3.01	1009.21	2.65	0.00	84.18
reheater_2_deaerator	277.58	6.19	1224.12	3.05	0.00	100.20
lpt_in	285.01	1.32	3010.20	6.93	1.00	1331.44
lpt_stg1	136.69	0.29	2733.16	7.03	1.00	297.92
lpt_out	43.70	0.01	2281.01	7.24	0.88	1033.52
cond_mix	43.71	0.01	182.99	0.62	0.00	1331.44
cpump	43.75	1.32	184.36	0.62	0.00	1331.44
lpfwh	128.90	1.32	542.35	1.62	0.00	1331.44
fwpump_suction	167.63	1.32	709.06	2.02	0.00	2003.99
fwpump	168.25	6.19	714.57	2.02	0.00	2003.99
hpfwh	223.90	6.19	962.68	2.55	0.00	2003.99
hpfwh_stm_out	234.04	3.01	1109.54	2.85	0.06	315.52
deaerator_hpfwh_stm	192.24	1.32	1109.54	2.88	0.15	315.52
lpfwh_stm_out	132.16	0.29	1133.24	3.08	0.27	297.92
cond_fw	43.70	0.01	1133.24	3.62	0.40	297.92

2.1.2 Simulink Reduced-Order PWR-TPD Simulator

While the Python RO model is limited to simulating the system's quasi-steady state response, the Simulink model, with a more realistic representation of system components, can simulate the transient process. The Simulink model includes detailed representations of turbines, heat exchangers, and extraction flows, which are based on pressure differences across nodes. The system components are modeled to replicate the steady-state response for 0% TPD, as outlined in Table 1.

This initial version of the Simulink model does not feature a closed-loop control system capable of regulating system variables across different TPD levels. As a result, the control setpoints identified from the Python RO model are used in a lookup table to adjust system variables. These controls include regulating the feedwater flow rate to maintain a thermal power absorption of 3646.88 MWt from the primary side, adjusting the turbine valve opening to maintain the pressure header at the rated 6.19 MPa, controlling the flow for the TPD system, managing the steam flow toward reheater 2, and regulating the operating pressures of the condenser, deaerator, and moisture separator. The extraction flow rates from turbines are determined by flow resistances. Figure 2 provides the screenshot of the TPD-PWR model in Simulink.

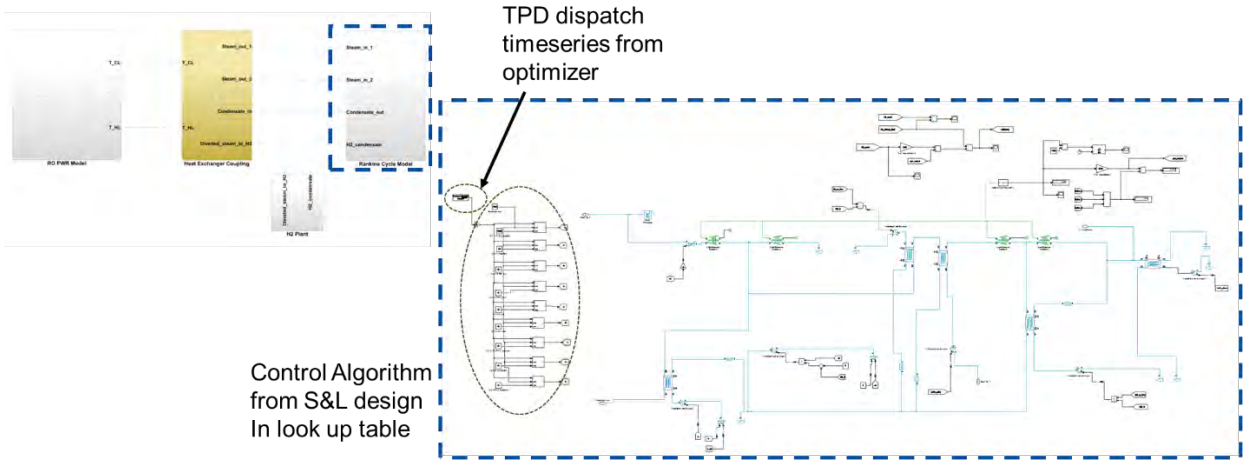

Figure 2. Real-time transient process model of Simulink PWR-TPD simulator.

2.1.3 Model Comparison and Validation

2.1.3.1 Steady State Response

Figure 3 (a)-(c) compare the turbine power output, main steam flow rate, and feedwater temperature predictions of the PWR-TPD models with the values reported for 0%, 30%, 50%, and 70% TPD levels by S&L [6]. Using the initialization sequence, the Python model was simulated for TPD levels ranging from 0% to 70% at 0.1% intervals. In contrast, the Simulink model was simulated only for 0%, 30%, 50%, and 70% TPD levels, as it requires transient simulations to arrive at steady-state solutions for a given TPD level.

The turbine power output from both the Python RO model and the Simulink model shows a similar decreasing trend with increasing TPD%, consistent with the S&L PEPSE model. Both RO models also exhibit the same turbine power output at 0% TPD, which is lower than the value reported by S&L. However, as TPD% increases, the discrepancy between the Python RO model and the S&L model decreases. The Simulink model, however, predicts slightly higher turbine power output than the S&L model for TPD levels greater than 30%.

Regarding feedwater temperature, both RO models show significant discrepancies compared to the S&L model. This is expected, as the S&L model incorporates detailed multi-stage turbine extractions and

multistage feedwater heaters, while the PWR-TPD models use a turbine steam extraction and feedwater heater design. Nevertheless, the Simulink RO model predicts feedwater temperature more accurately than the Python RO model. The main steam flow predictions from the Python RO and Simulink RO models are close to each other, except at 30% TPD, though both deviate significantly from the values reported by S&L.

As noted above, the control of the Simulink RO model is based on a lookup table populated with control setpoints predicted by the Python RO model. While the amount of reactor thermal power delivered to the secondary coolant and the steam header pressure are maintained at their rated conditions, other variables are not necessarily maintained at their target values. For instance, since the Simulink model's feedwater inlet temperature is higher than that of the Python model, and the main steam flow rates are nearly the same, the same thermal input means the Simulink model will have slightly superheated steam at the outlet of steam generator. This explains the increased turbine power output observed in the Simulink model as compared to the Python RO model.

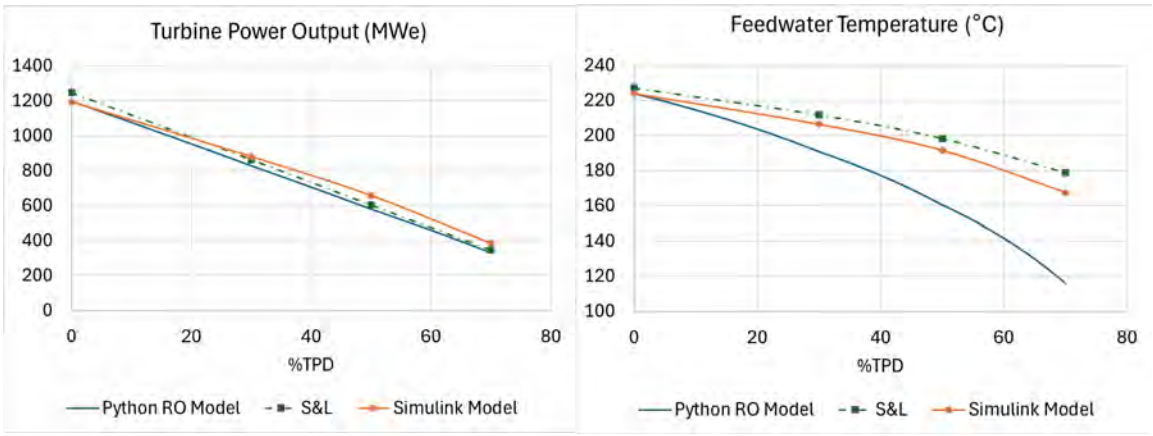

(a) (b)

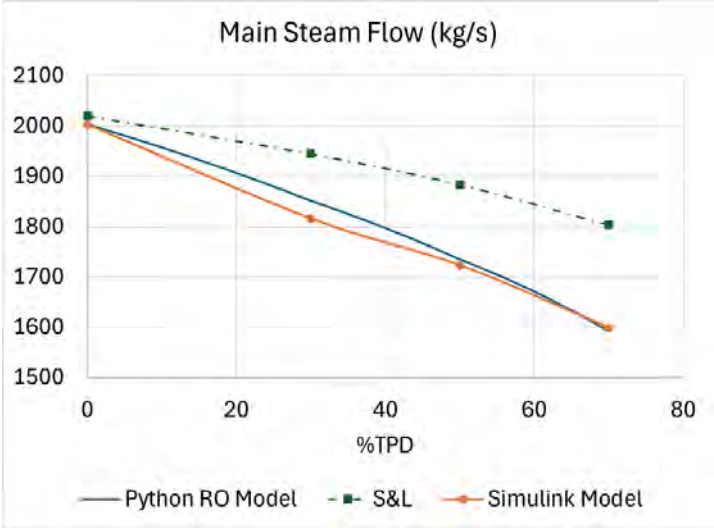

(c)

Figure 3. Comparison of steady-state responses of the selected PWR-TPD models.

2.1.3.2 Dynamic Response

While the Python RO model is limited to predicting the system's quasi-static behavior, the Simulink RO model can simulate the system's transient operation, particularly during changes in TPD extraction. We analyzed the system's response when switching from 0% to 30% TPD and from 30% TPD back to 0%. Although the system is capable of simulating transients at higher TPD extraction levels, a 30% TPD analysis is sufficient, considering that SOEC hydrogen production requires less than 10% of the rated reactor thermal power in the form of heat delivery.

In this simulation, the system switches from 0% TPD to 30% TPD during a period of approximately 5.5 hours. As expected, steam flow to both the HP and LP turbines decrease with increasing TPD, as shown in Figure 4. Notably, the pressure at the inlet of the HP turbine decreases from 5.53 MPa at 0% TPD to just under 4 MPa at 3% TPD, and the feedwater temperature entering the steam generator decreases from 224°C to 201°C because as main steam is diverted to TPD and the pressure in the turbines decrease, less steam is extracted from the turbines to support feedwater heating. The decrease in feedwater temperature with increasing TPD causes the total steam flow in the main steam line to decrease with increasing TPD, so that the saturation temperature and pressure can be maintained in the steam generator with a fixed amount of reactor heat.

The net system efficiency, which represents the efficiency of heat utilization in both thermal extraction and turbine operation, improves as more heat is diverted to the thermal process. These results indicate the Simulink PWR-TPD simulator adequately captures the overall trends of electric and thermal power dispatch during transient TDP operations.

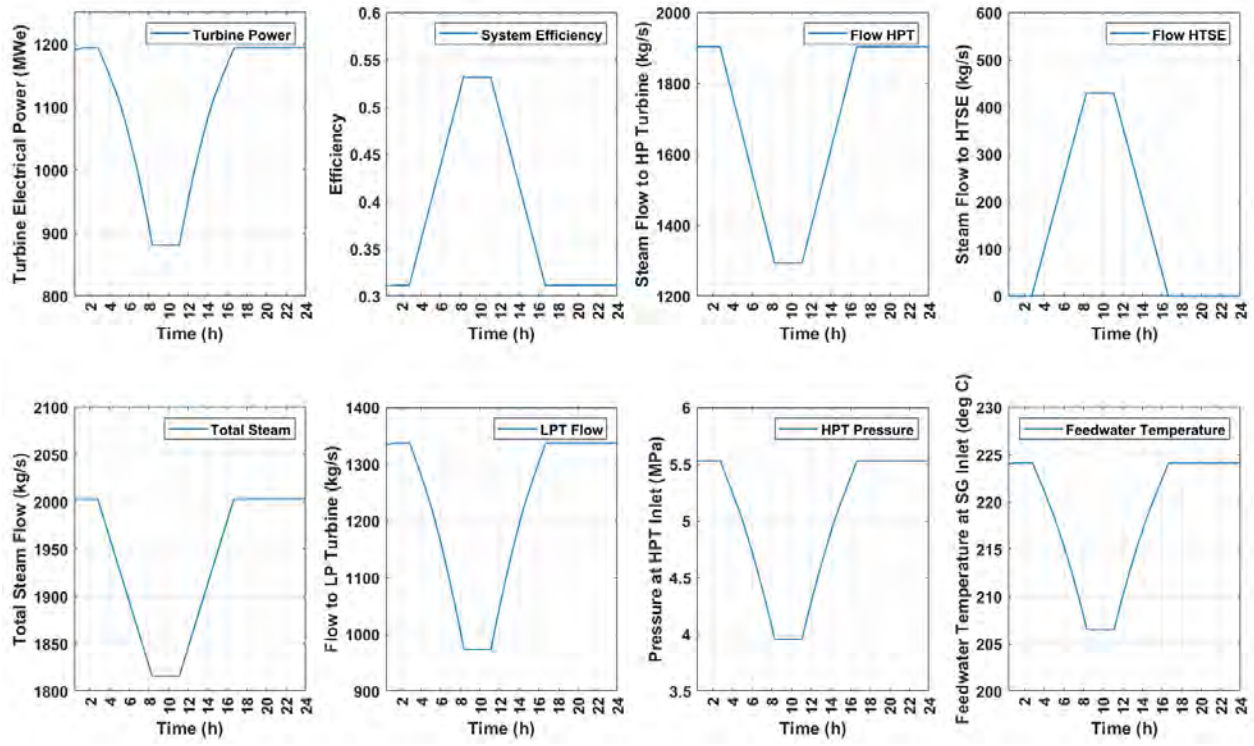

Figure 4. Transient response of Simulink PWR-TPD simulator variables during transitions from 0% TPD to 30% and back to 0%.

2.2 High Temperature Steam Electrolysis

This section briefly describes the dynamic model of a SOEC plant system developed in MATLAB/Simulink. The plant model includes 2 main modules which include the balance of plant (BoP) and the SOEC stack module. The BoP module consists of the heat exchangers, pumps, reservoirs and topping heaters. The thermal power used to convert water to steam is extracted from the nuclear power plant. The coupling between the NPP thermal extraction and HTSE is through a heat exchanger. The temperature of the steam entering the system (supplied by the nuclear plant) is approximately 130°C. The temperature of the incoming stream is increased through recuperated heat from the product hydrogen-steam mixture by heat exchangers and also by electric topping heaters to 750°C before it is delivered to the electrolysis cells. On the airside of the BoP, incoming air is heated using heat recuperated from the oxygen-enriched air product and by electric heaters to increase it to 750°C before it is delivered to the electrolysis cells. The simplified process flow diagram of the SOEC system is shown in Figure 5, which also includes a DC power delivery system and hydrogen compressor.

The SOEC stack model has 3 submodules that mimic the electrical dynamics, the fluid dynamics, and the thermal dynamics of SOEC stacks. The electrical dynamics submodule outputs the dynamic cell voltage behavior based on the cell's electrochemical double-layer phenomenon. The fluid dynamics submodule outputs the dynamic behavior of the average partial pressure conditions of the reaction based on the pressure inertia due to finite flowrates and inlet/outlet flow rate conditions of the stack based on the feed factors. The thermal dynamics submodule outputs the dynamic behavior of average stack temperature and the inlet stream temperature based on the SOEC thermal dynamics and preheater thermal dynamic, respectively.

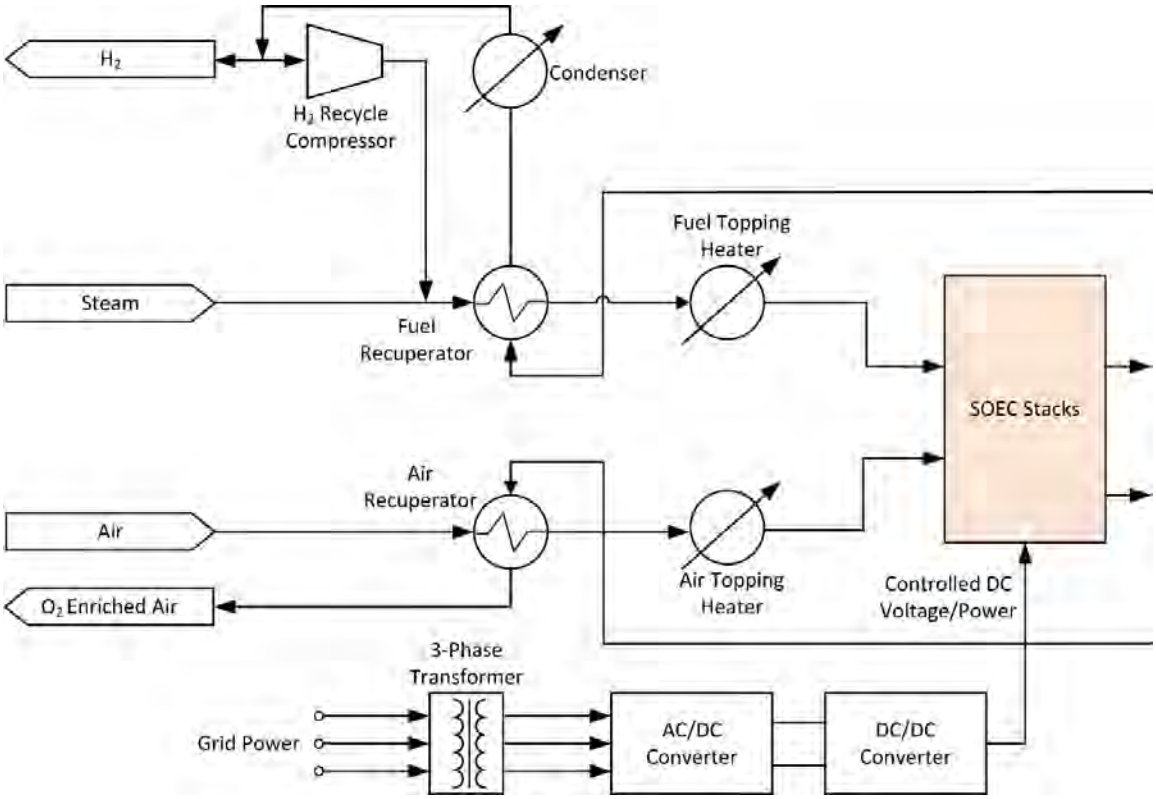

Figure 5. Schematic of the High Temperature Steam Electrolysis System.

3. OPTIMIZATION FORMULATION CONSIDERING RESERVE SERVICES

3.1 Nomenclature

Index (represented as a subscript)

t	Index of time periods

Sets (represented as subscripts after parameter symbols)

G	Generators
H	High-temperature electrolysis
I	Integrated energy system
T	Scheduling horizon
B	Balance of Plant
S	Electrical grid

Parameters

$P_i^{max\,/min}$	Maximum/minimum electric power production from component i, MW.
$R_i^{U/D}$	Ramp up/down rates of component i, MW.
$C_{E,t}$	Electricity price, $\$/MWh$.
$C_{SR,t}$	Synchronized reserve market clearing price, $\$/MW$.
$C_{PR,t}$	Primary reserve market clearing price, $\$/MW$.
$C_{TR,t}$	Thirty-minute reserve market clearing price, $\$/MW$.
Q_{cs}	Rated thermal power of steam generator, $\$/MW$.
$Q_i^{max/min}$	Maximum/minimum thermal power consumption by component i, $\$/MWt$.
m_H	Hydrogen demand during the scheduling, kg.
$\eta_{t/g}$	Turbine/generator efficiency.
Δ_t	Simulation time step, hours.

Variables

$SR_{i,t}$	Synchronized reserve provided by component i during interval t, MW.
$PR_{i,t}$	Primary reserve provided by component i during interval t, MW.
$TR_{i,t}$	Thirty-minute reserve provided by component i during interval t, MW.

$\dot{m}_{H_2,t}$	Hydrogen production rate, kg/s.
$P_{i,t}$	Electrical power consumed/generated by component i, MWe.
$P_{mech,t}$	Mechanical power, MW.
$Q_{i,t}$	Thermal power consumed by component i, $MWth$.
$r_{PR,t}$	Revenue due to primary reserve during interval t, $.
$r_{SR,t}$	Revenue due to synchronized reserve during interval t, $.
$r_{TR,t}$	Revenue due to thirty-minute reserve during interval t, $.
$r_{E,t}$	Revenue due to energy during interval t, $.
$r_{tot,t}$	Combined revenue of energy and reserves during interval t, $.
$r_{H,t}$	Revenue due to hydrogen during interval t, $.

3.2 Energy market modeling

3.2.1 LWR

The LWR integrated energy system (IES) comprises three subsystems: Light Water Reactor (LWR), High-temperature Steam Electrolysis (HTSE), and Balance of Plant (BoP). The LWR employs nuclear fission to produce high-temperature steam, which is then directed to the turbine and the HTSE unit. Operations within the IES are governed by the thermal energy balance constraint in which heat from the steam generator (Q_{cs}) equals the sum of heat dispatched to the hydrogen plant ($Q_{H,t}$) and heat delivered to the LWR BoP ($Q_{B,t}$):

$$Q_{H,t} + Q_{B,t} = Q_{cs} \tag{1}$$

3.2.2 Balance of Plant

In the BoP configuration, a steam turbine is coupled with a synchronous generator. The turbine transforms the thermal energy into mechanical power:

$$P_{mech,t} = \eta_t Q_{B,t} \tag{2}$$

where η_t is the LWR thermal efficiency. Subsequently, this mechanical power is converted to electricity:

$$P_{G,t} = \eta_g P_{mech,t} \tag{3}$$

where η_g is the efficiency of the generator. The electricity output from the generator must stay within the predefined operational limits:

$$P_G^{min} \leq P_{G,t} \leq P_G^{max} \tag{4}$$

Additionally, the generator adheres to specific ramp-up and ramp-down rates:

$$P_{G,t} - P_{G,t-1} \leq R_G^U \tag{5}$$

$$P_{G,t-1} - P_{G,t} \leq R_G^D \tag{6}$$

3.2.3 High-temperature Steam Electrolysis (HTSE)

The HTSE utilizes both heat ($Q_{H,t}$) and electricity ($P_{H,t}$) to produce hydrogen. The consumption rates of heat and electricity are proportional to the hydrogen production rate, expressed by:

$$Q_{H,t} = k_{q1}\ \dot{m}_{H_2,t} \tag{7}$$

$$P_{H,t} = k_{p1}\dot{m}_{H_2,t} \tag{8}$$

The HTSE operates within a predefined electrical range:

$$\mathrm{P_H^{min}} \leq \mathrm{P_{H,t}} \leq \mathrm{P_H^{max}} \tag{9}$$

It also follows specific ramp-up and ramp-down rates:

$$P_{H,t} - P_{H,t-1} \leq R_H^U \tag{10}$$

$$P_{H,t-1} - P_{H,t} \leq R_H^D \tag{11}$$

Over the scheduling horizon T, the actual hydrogen production is required to meet or exceed the hydrogen demand:

$$\sum_{t\in T} \dot{m}_{H_2,t}\,\Delta_t \geq m_H \tag{12}$$

3.2.4 Electrical Grid

The generator provides electricity to the HTSE unit, and surplus electricity is sold to the electrical grid:

$$\mathrm{P_{H,t}} + \mathrm{P_{S,t}} = \mathrm{P_{G,t}} \tag{13}$$

3.3 Ancillary market modeling

This subsection details the operational constraints in the ancillary service market of the PJM Interconnection, focusing on the reserve types available in the day-ahead market.

Three kinds of reserves are discussed: primary, synchronized, and 30-minute reserves. The power from primary and synchronized reserves is required within 10 minutes of a request, while power from the 30-minute reserve should be available within 30 minutes. Note that the day-ahead market in PJM does not offer regulation services.

3.3.1 Real Power Maximum Limit

For the generator, the power output ($P_{B,t}$) plus the capacity allocated for synchronized reserves ($SR_{G,t}$), primary reserves ($PR_{G,t}$), and 30-minute reserves ($TR_{G,t}$) must not exceed its maximum allowable operating limit:

$$P_{G,t} + SR_{G,t} + PR_{G,t} + TR_{G,t} \leq \min(P_G^{max}, \eta_t\,\eta_g\ Q_G^{max}) \tag{14}$$

where $Q_G^{max} = Q_{cs} - Q_H^{\min}$ represents the maximum thermal power delivered to the turbine.

3.3.2 Real Power Minimum Limit

The power consumption of the hydrogen plant must not fall below its minimum operational threshold, accounting for power that is dispatched to meet primary, synchronized and 30-minute reserve commitments:

$$P_{H,t} - PR_{H,t} - SR_{H,t} - TR_{H,t} \geq P_H^{min} \tag{15}$$

3.3.3 Ramp-Up Limits

The generator's increase in power output plus the reserve allocations must not exceed its ramp-up capacity:

$$P_{G,t} + PR_{u,G,t} + SR_{G,t} + TR_{G,t} - P_{G,t-1} \leq R_G^U \tag{16}$$

3.3.4 Ramp-Down Limits

The power ramp down rate of the hydrogen facility must not exceed its ramp-down capacity, accounting for dispatched reserves:

$$\mathrm{P_{H,t-1}} - \left(\mathrm{P_{H,t}} - \mathrm{PR_{H,t}} - \mathrm{SR_{H,t}} - \mathrm{TR_{H,t}}\right) \leq \mathrm{R_H^D} \tag{17}$$

3.3.5 Synchronized Reserve of IES

The synchronized reserve for the IES is the combined synchronized reserves from the LWR generators and the hydrogen facility:

$$SP_{G,t} + SP_{H,t} = SP_{I,t} \tag{18}$$

3.3.6 Primary Reserve of IES

The primary reserve of the IES is the combined primary reserves from the LWR generators and the hydrogen facility:

$$PR_{G,t} + PR_{H,t} = PR_{I,t} \tag{19}$$

3.3.7 Thirty-minute Reserve of IES

The thirty-minute reserve of the IES is the sum of the thirty-minute reserve from the LWR generators and the hydrogen facility:

$$TR_{G,t} + TR_{H,t} = TR_{I,t} \tag{20}$$

3.3.8 Ancillary Service Revenue

The revenue from ancillary service is the aggregate of payments for reserves, calculated based on the clearing prices of the awarded reserves. The total payment formula is given by:

$$r_{CR,t} = \sum_{t \in T} (SR_{I,t} C_{SR,t} + PR_{I,t}\, C_{PR,t} + TR_{I,t}\, C_{TR,t}) \tag{21}$$

3.4 Model Formulation

The operation of IES can be modeled as a linear programming problem. This model aims to maximize total revenues derived from both energy and ancillary markets. Simultaneously, it ensures that all subsystems adhere to their specific operational constraints. The optimization problem for the IES can be written as [21]:

$$\max \Delta t \sum_{t=1}^{T} \left(c_{E,t} \times \frac{P_{s,t}}{3600} + r_{CR,t} \right) \tag{22}$$

4. SIMULATION RESULTS

4.1 Simulation setup

Electricity and ancillary services are dispatched hourly, while other decision variables within the IES, such as hydrogen production rates, are determined every 5 minutes. The operation horizon T for the model is set at 24 hours. Energy and reserve prices for the node PJM-RTO on May 14th, 2024, in the Pennsylvania-New Jersey-Maryland Interconnection (PJM) market are illustrated in Figure 6 (Interconnection, 2024). Energy prices are significantly higher than reserve prices. Hydrogen demand is set at 80% of the maximum production capacity of the hydrogen facility.

To assess the economic performance of the IES from the electricity market, a 24-hour simulation is conducted in which the IES participates in both energy and ancillary service markets. Assuming acceptance of the IES's reserve offer by PJM, we analyze the potential dispatch of energy and reserves. The optimization model, developed in Python using Pyomo and solved with CPLEX, runs on a laptop equipped with 10 cores and 16 GB of RAM.

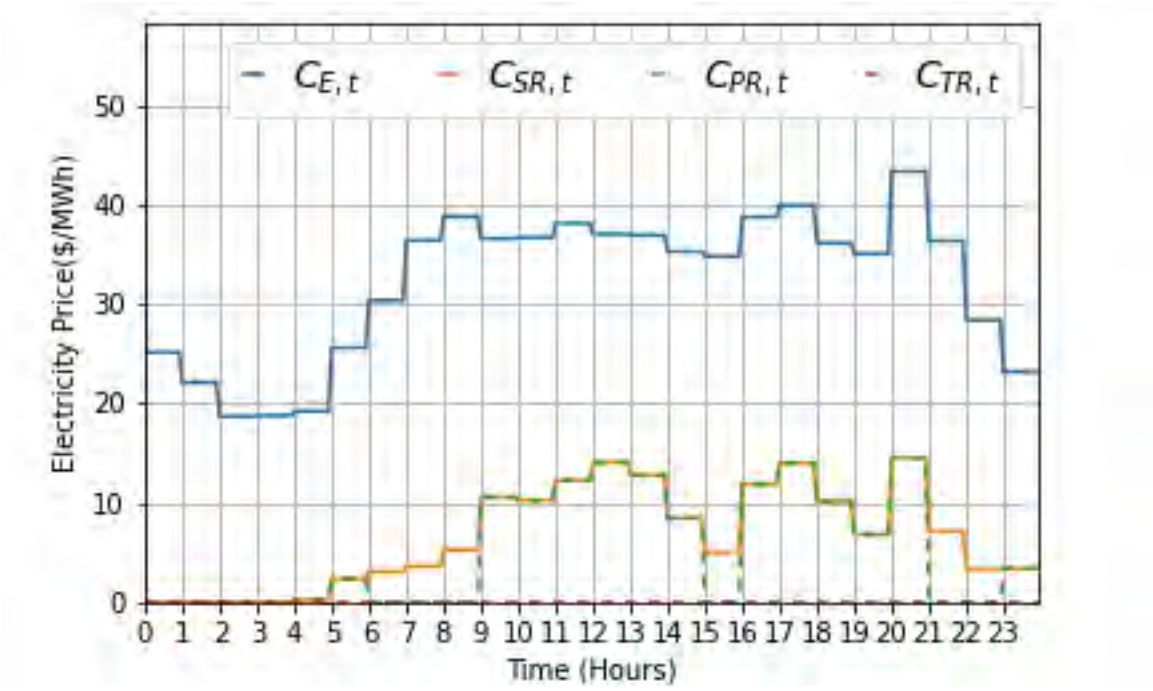

Figure 6. An overview of 24 hours of electricity price ($C_{E,t}$), primary reserve clearing price ($C_{PR,t}$), synchronized reserve clearing price ($C_{SR,t}$), and thirty-minute reserve clearing price ($C_{TR,t}$).

4.2 Optimization Results

Figure 7 illustrates the electricity output from the LWR generators, consumption by hydrogen facility, and electricity sold to the grid. The electricity consumption by hydrogen facility plus electricity sold to the grid equals the generator output. A prominent feature in Figure 7 is that when the hydrogen facility curtails production to its minimum level, the power produced by the LWRS generator increases. The cause of this behavior is that curtailment of hydrogen production increases the flow of steam to the LWR turbine-generator system, so that it can produce maximum power. Electricity sold to the grid is at its lowest when energy prices are lowest, between hours 0 to 7 and after hour 22.

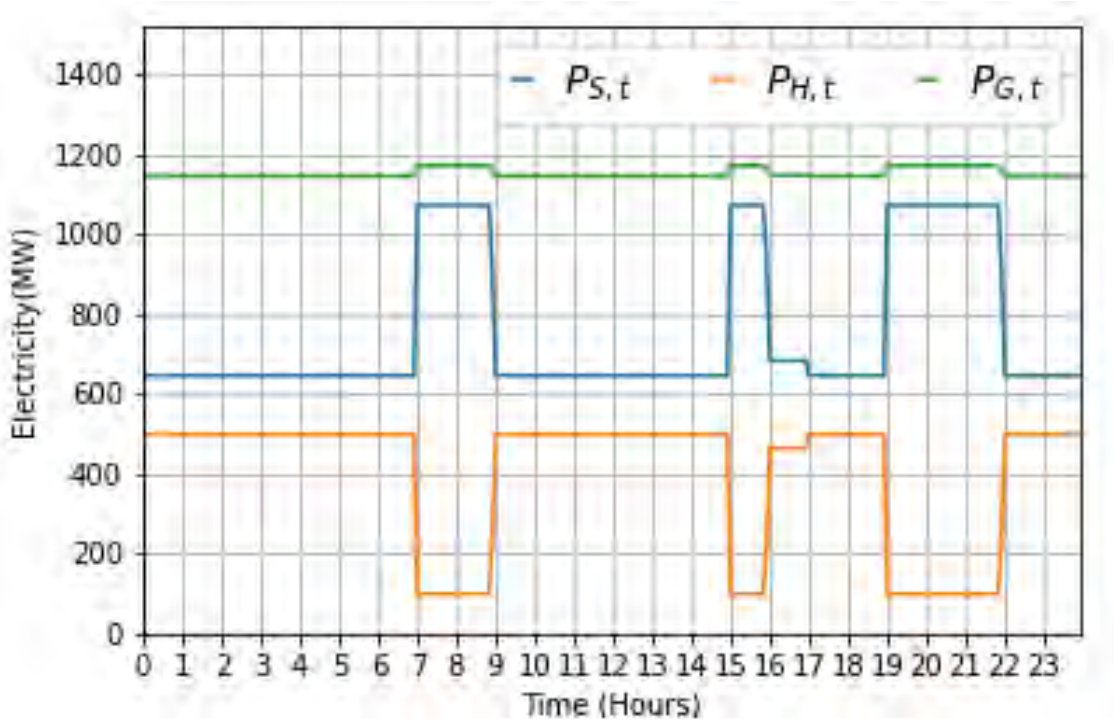

Figure 7. Electricity outputs of the generator ($P_{G,t}$) and electricity consumption by hydrogen facility ($P_{H,t}$), and surplus electricity sold to the electrical grid ($P_{S,t}$).

Figure 8 displays the dispatch of energy and reserve. The total reserves are sourced from hydrogen production. Specifically, between hours 0 and 1, the total is $425.89\ MW$, where $400\ MW$ is derived from the ramp-down capability of hydrogen facility, and $25.89\ MW$ is additional electricity output from the generator due to reduced heat consumption by the hydrogen facility. The absence of dispatch for the 30-minute reserve results from its zero-market clearing price. Figure 9 presents revenue details for every 5-minute interval, encompassing hydrogen, the combined total of energy and reserve, energy alone, synchronized reserve, and primary reserve. It does not include the revenue for the 30-minute reserve, as it is zero. Compared with participating only in the energy market, engaging in both markets increases the 24-hour revenue from $599,812.47 to $644,641.76, an increase of 7.4%.

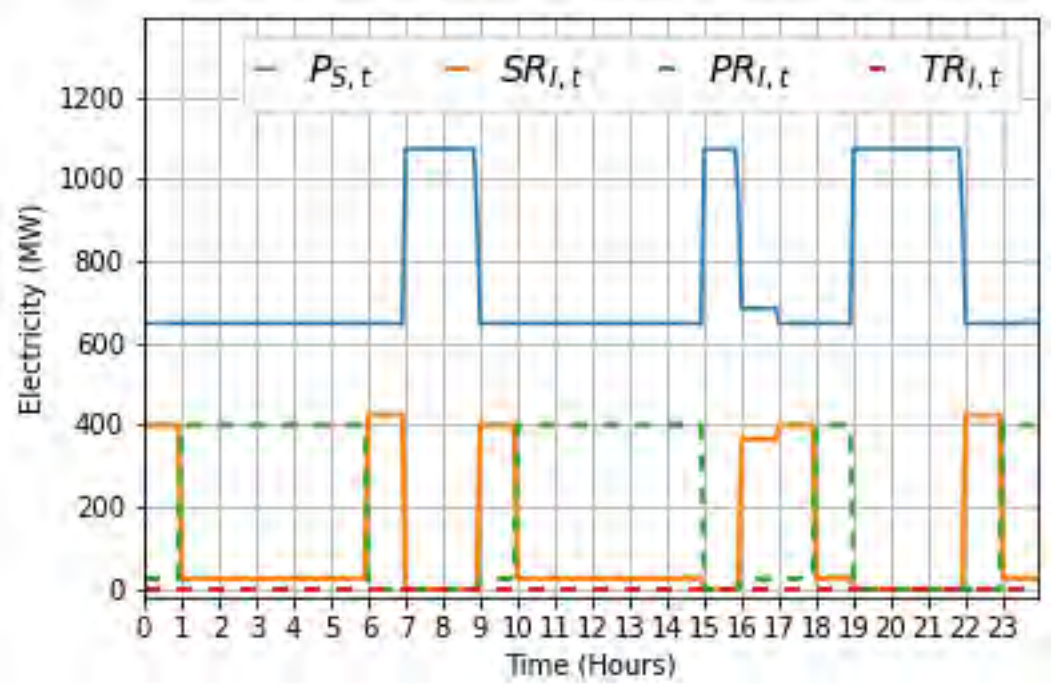

Figure 8. Dispatch for electricity ($P_{S,t}$), primary reserve ($PR_{i,t}$), synchronized reserve ($SR_{i,t}$), and thirty-minute reserve ($TR_{i,t}$) over 24 hours.

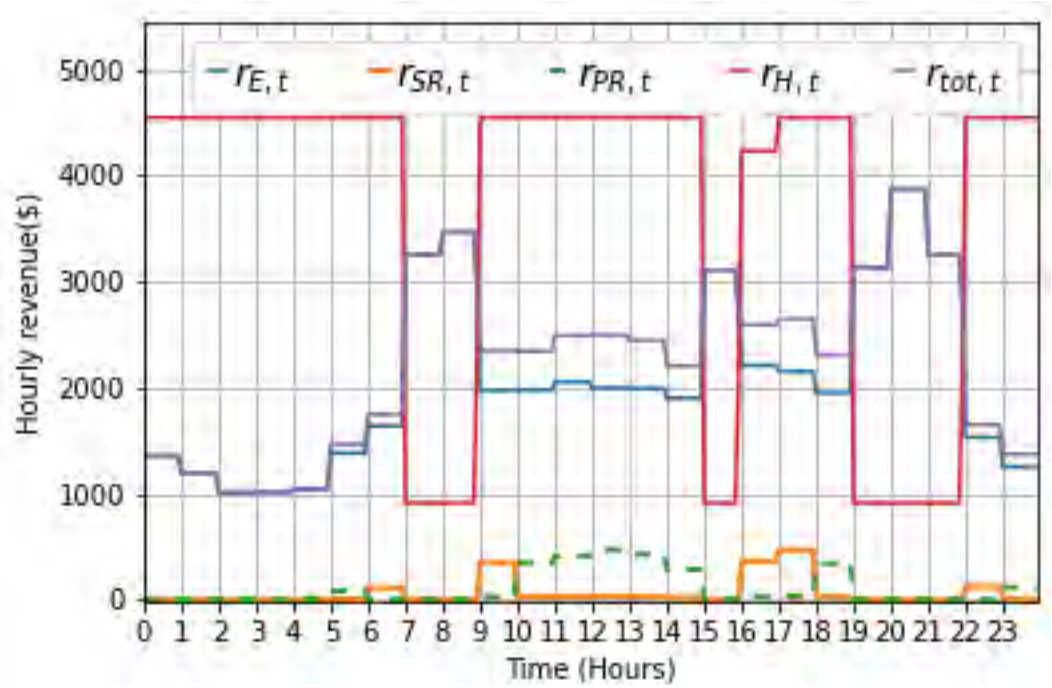

Figure 9. Revenue on 5-minute intervals, including hydrogen ($r_{H,t}$), the combined total of energy and reserve ($r_{tot,t}$), grid electricity ($r_{E,t}$), synchronized reserve ($r_{SR,t}$), and primary reserve ($r_{PR,t}$) over 24 hours.

4.3 Real-Time Simulation Results

To evaluate the grid dynamics based on the dispatch setpoints obtained from the proposed optimization formulation for electricity and ancillary services, the generation resource (nuclear power plant) and the hydrogen facility are modeled and integrated on the well-known IEEE 39 New England transmission network, which is shown in Figure 10. The IEEE 39-bus network, which is commonly referred to as the 10-machine New England system, provides a benchmark grid for simulating the dynamic behavior of a representative electric power grid under various conditions to explore reliability, stability, and optimal power flow, as well as economic dispatch. The system consists of 10 generators, as well as several bus loads, transmission lines and capacitor banks.

The nuclear power plant is represented as Gen 1 on the network. The hydrogen facility (HTSE plant) is modeled as an in-house load connected to the nuclear power plant, such that the power injection on bus 39 will always be the net power $P_{S,t}$ and is expressed as

$$P_{S,t} = P_{G,t} - P_{H,t} \quad (23)$$

A 500 MW solar resource is modelled and integrated as Gen 10 on bus 30 of the network. The modified IEEE 39-bus system is modeled in RSCAD using a Real-time digital simulation platform.

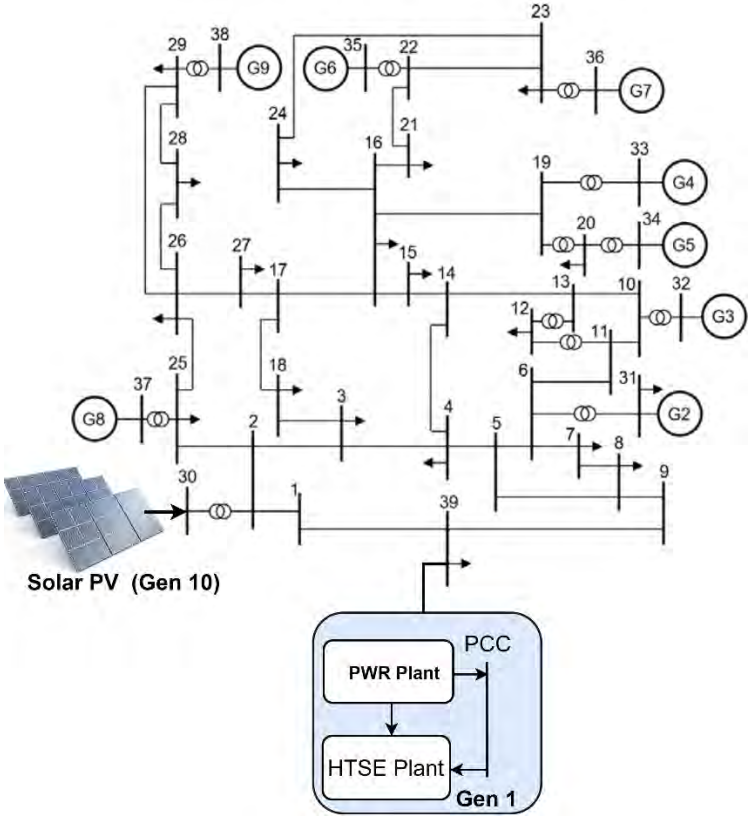

Figure 10. IEEE 39-bus New -England System.

4.3.1 Grid Response

The uncertain and stochastic power generation of the solar plant challenges the ability of the grid to maintain reliability. The optimal power flow by the utility is based on the forecasted solar power generation, such that during real-time operation, the solar power generation will vary from the forecast resulting in forecast error. The forecast and the actual power generation by the solar power plant is shown in Figure 11. Within the constraints of hydrogen production and ramping, hydrogen production is

modulated to address the difference between the forecasted solar power and the real-time solar power generation to facilitate greater penetration of solar power on the grid, as shown in Figure 12. During the periods where the actual dispatch of the solar PV plant is less than the forecasted, hydrogen production can be curtailed to make up for the lower-than-expected power generation.

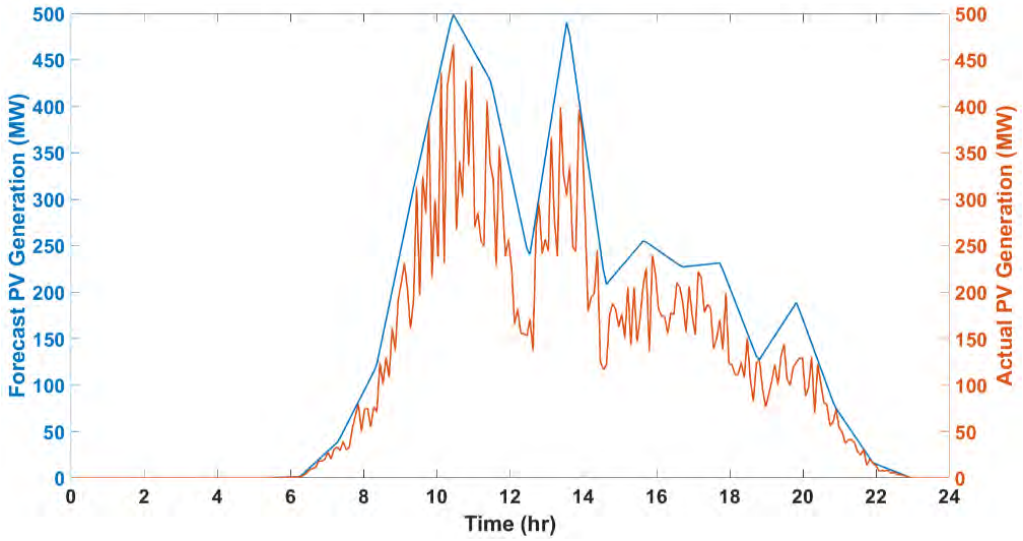

Figure 11. Solar power plant forecast and actual power generation.

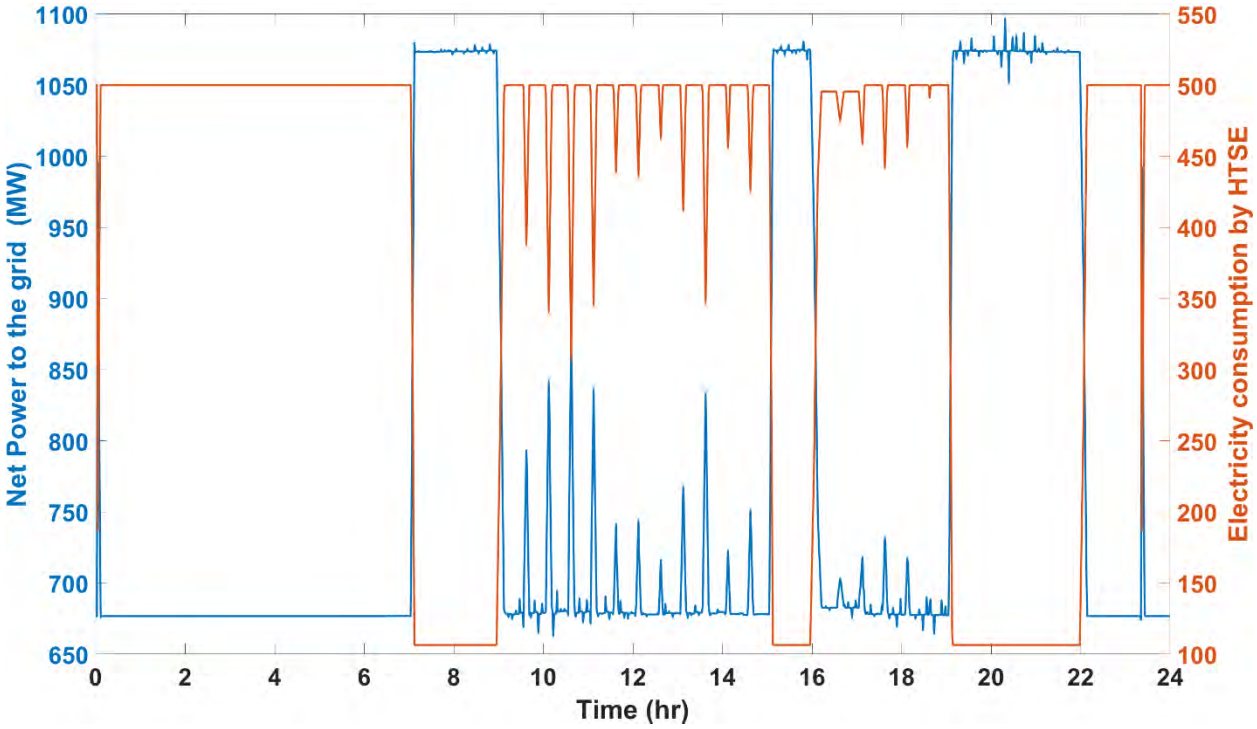

Figure 12. Modulated hydrogen facility dispatch and net electricity sold to the grid by the IES (to balance variable solar power generation).

The dynamic grid response to changes in electricity dispatch by the nuclear power plant is shown in Figure 13. The nominal bus voltage of the IEEE 39 bus network is 345 kV, and its nominal frequency is 60 Hz. Measurements taken from the point of interconnection (POI) of the nuclear power plant show that

during the real time simulations, the system voltage and frequency are well within acceptable limits. The voltage is well within the 0.95-1.05 pu (the minimum and maximum voltages are 340 kV and 345.5 kV, respectively) and the frequency is well within 59.5-60.5 Hz. These results indicate the IES can effectively participate in providing ancillary services without causing voltage or frequency stability issues in the grid.

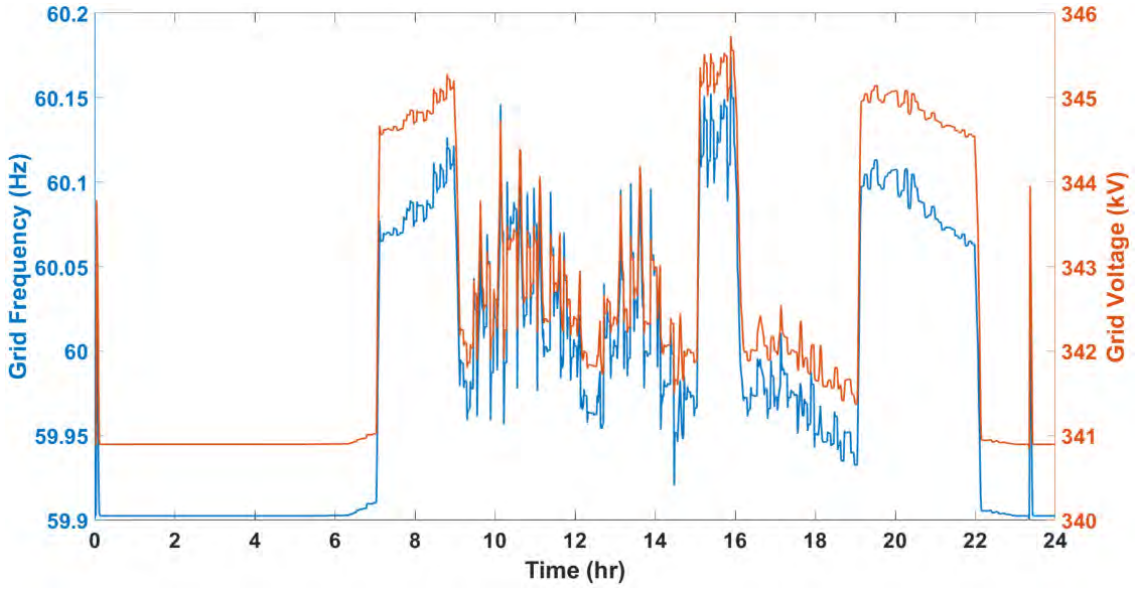

Figure 13. Dynamic grid voltage and frequency response during the real-time digital simulation.

4.3.2 Reactor and Thermal System Response

Most of the energy required for hydrogen production is supplied by electricity. Under nominal conditions, the hydrogen facility demands 500 MWe of electricity and 100 MWt of heat, with the 100 MWt representing 2.74% of the reactor's rated thermal power.

Figure 14 and Figure 15 show the reactor's thermal and secondary coolant dynamics during the 24-hour simulation. As previously discussed, the control system for the Simulink RO-PWR-TPD simulator, which is based on interpolating pre-calculated control setpoints in a lookup table, does not provide precise control for intermediate extraction levels between 0%, 30%, 50%, and 70% TPD. With 2.74% TPD during nominal hydrogen production, the reactor's thermal power experiences a slight deviation ~18 MWt from the rated 3646.88 MWt. At reduced hydrogen production, the thermal power dispatch is lower than 2.74% and the deviation of thermal power is also lower.

Initially, the reactor operates at 3665 MWt during full hydrogen production, with ~40 kg/s of steam extracted for the process. Between hours 7-9, the optimizer commands the system to reduce hydrogen production to its minimum value (20% of the maximum rating capacity) in response to pricing signals, leading to a decrease in steam extracted for hydrogen production and an increase in total steam flow. A slight reduction in reactor thermal power is observed, and the plant's electrical output rises slightly. Between hours 9 and 15, the optimizer commands hydrogen production to return to 100% production and commit to provide grid reserves. This period coincides with expected peak solar generation; however, due to lower-than-forecast solar output, the grid decides to utilize a part of reserve committed by the IES. As noted above in connection with Figure 7, the total power produced by the LWR increases as hydrogen production decreases because dispatch of steam to the hydrogen plant is curtailed, allowing greater steam flow to the turbine system and consequently more power production.

Overall, the IES successfully provides reserve services by adjusting the hydrogen production setpoint in real time according to grid demand, without causing any significant transients in the reactor's primary system.

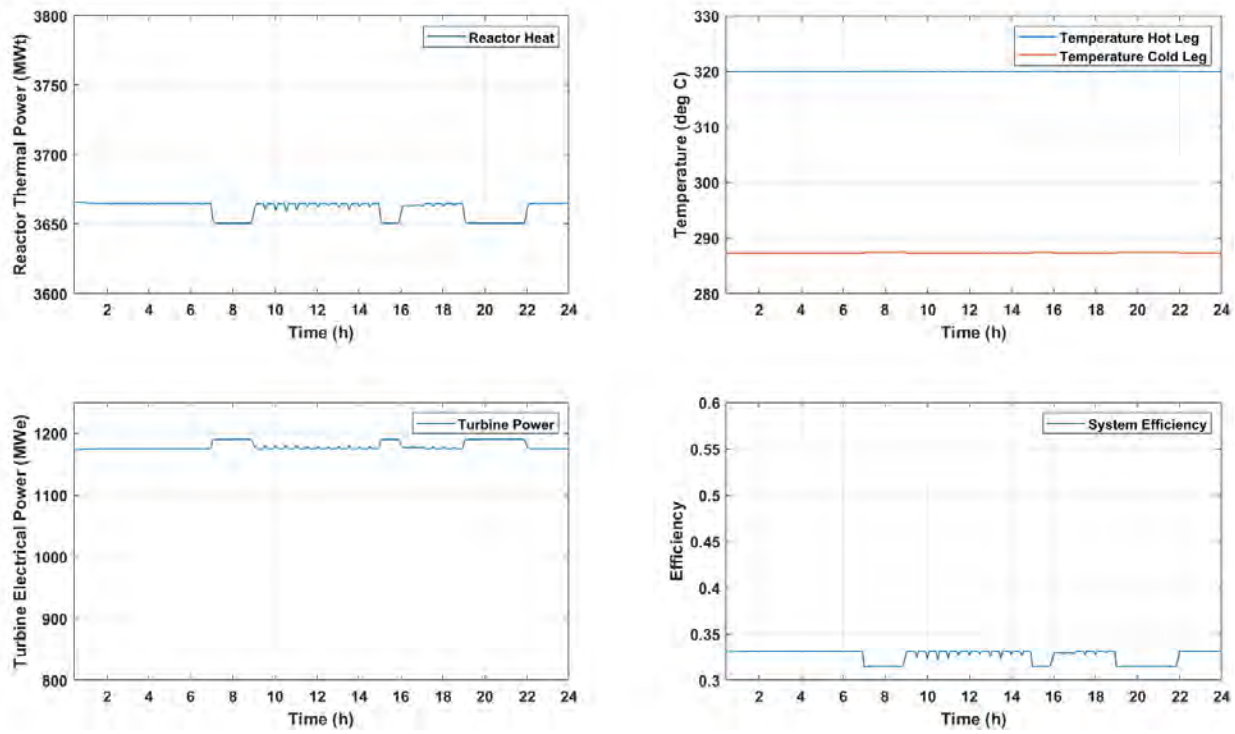

Figure 14. Reactor thermal power input, electrical power output and system efficiency for the given 24 h operation.

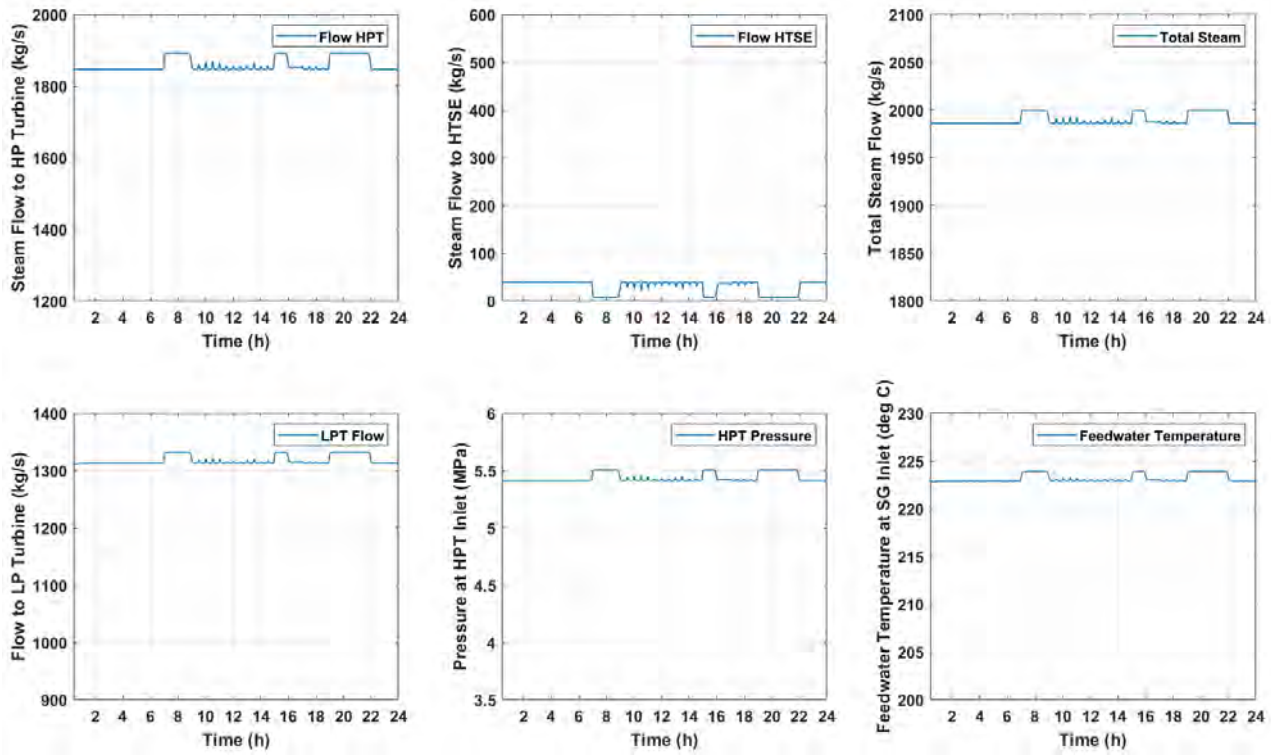

Figure 15. Flow rates, steam pressure and feedwater inlet temperature for the 24-h operation.

5. CONCLUSIONS AND FUTURE WORK

The integration of LWRs with high-temperature steam electrolysis hydrogen production offers a promising pathway to enhance the role of nuclear energy in a decarbonized energy system. LWRs can dynamically allocate thermal power between electricity generation and hydrogen production, providing significant grid benefits by offering both spinning and non-spinning reserve capacities.

In this report, two models for the PWR-TPD system based on a 4-loop PWR design were discussed. A reduced-order (RO) Python model is capable of calculating steady-state responses and quasi-dynamic behavior of TPD transitions in faster-than-real-time scenarios. A corresponding dynamic RO Simulink model with detailed component models can predict transient behavior during TPD transitions. Due to the complex and non-linear nature of the thermal hydraulic system, precise control of the thermal dispatch system requires an advanced control system to manage transitions between the different TPD levels, which may be implemented in future work. Both the Python and Simulink simulators can integrate with real-time digital simulation platforms (e.g., RTDS) and optimization algorithms to provide real-time analysis of system operations. The behavior of the PWR-TPD simulators were compared with high-fidelity results generated by Sargent and Lundy using a detailed PEPSE model of 4-loop Westinghouse PWR. While both models predicted turbine power output with acceptable accuracy, clear discrepancies were found in the predicted feedwater flow rate and feedwater inlet temperature. These discrepancies mainly arise from simplifications in the PWR-TPD models.

An optimization algorithm was developed that considers the system's ability to provide flexible thermal dispatch while supporting both electricity demand and reserve ancillary services. Hydrogen production is flexibly dispatched to meet day-ahead and real-time electricity demand and ancillary service market demands while compensating for variable solar power. For a system connected to the PJM market, optimization results show that participating in both reserve and regulation markets increases daily

revenues by 7.5%, while still adhering to contracted daily hydrogen production constraints. This approach not only makes the system more dynamic and responsive to grid pricing signals but also enables the nuclear power plant to improve grid reliability by providing ancillary services. Additionally, it leverages the reactor's capabilities more efficiently. Supplementary analysis at the end of the report includes optimization results for the CAISO market, which has compensation structures for both reserve and regulation services, as well as for the integrated energy systems with low-temperature electrolysis, which does not involve thermal power dispatch for hydrogen production.

Real-time simulations using an IEEE 39-bus systems demonstrate the deployment of reserves committed during optimization, accounting for inaccuracies in predicting solar PV generation. leading to a mismatch between dispatched generation and demand, prompting the grid to utilize the reserves provided by the integrated nuclear and hydrogen plants. The real-time results show that providing ancillary services by the IES has no adverse impact on the stability of the overall system and could potentially be used to improve grid stability. The minimum and maximum simulated voltages at the POI of the nuclear power plant during a 24-hour simulation were 340kV and 345.5kV, respectively. The minimum and maximum simulated frequencies at the POI of the nuclear power plant were 59.9 Hz and 60.15 Hz respectively.

The nuclear plant behavior during the 24-hour simulation shows that the system can handle TPD transitions and execute reserve services when requested by the grid without any significant transients affecting reactor operations.

Future work could include enhancing the reduced order Simulink PWR-TPD model by incorporating a closed-loop control system, conducting detailed multi-day and multi-timeframe operations of the integrated nuclear/hydrogen/renewable grid system, consideration of other ancillary services, including regulation and reactive power support, and performing real-time analyses of the system using actual ISO power system networks.

6. REFERENCES

[1]. H. Ritchie, “Sector by sector: where do global greenhouse gas emissions come from?,” Our World in Data, Sep. 2020. Accessed: Aug. 20, 2024. [Online]. Available: https://ourworldindata.org/ghg-emissions-by-sector

[2]. International Energy Agency (IEA), “World Energy Investment 2023,” Paris, France, May 2023. Accessed: Aug. 20, 2024. [Online]. Available: https://www.iea.org/reports/world-energy-investment-2023

[3]. United States Department of State, The Long-Term Strategy of the United States: Pathways to Net-Zero Greenhouse Gas Emissions by 2050. Washington DC, United States: United States Department of State and the United States Executive Office of the President, 2021. Accessed: Aug. 20, 2024. [Online]. Available: https://www.whitehouse.gov/wp-content/uploads/2021/10/US-Long-Term-Strategy.pdf

[4]. R. Lew, B. Poudel, S. Hancock, Y. Luo, T. L. Westover, “Development and Demonstration of a Reduced-Order PWR Power Dispatch Simulator,” Idaho National Laboratory, Idaho Falls, ID, United States, Tech. Rep. INL/EXT-21-63772, Aug. 2021. Accessed: Aug. 20, 2024. [Online]. Available: https://www.osti.gov/biblio/1905190

[5]. T. L. Westover, T. Olowu, S. Mahmud, A. Medam, Y. Ojo, and T. Ulrich, “Simulation of Power Dispatch from a PWR/SOEC System for Contingency Reserves,” Idaho Falls, Jun. 2023. Accessed: Aug. 20, 2024. [Online]. Available: https://lwrs.inl.gov/Flexible Plant Operation and Generation/PWR-CPD_Contingency-Reserves.pdf

[6]. T. L. Westover, J. Brown, F. R. Fidlow, H. Gaudin, J. Miller, K. Miller, G. Neimark, N. Richards, P. Kut, C. Paugh, “Light Water Reactor Sustainability (LWRS) Program Report: Preconceptual Designs of 50% and 70% Thermal Power Extraction Systems,” Idaho National Laboratory, Idaho Falls, ID, United States, Tech. Rep. INL/RPT-24-77206, Mar. 2024.
[7]. Pennsylvania-New Jersey-Maryland Interconnection, https://dataminer2.pjm.com/feed/da_ancillary_services/definition , accessed on: 2024-08-24.

7. SUPPLEMENTARY RESULTS

7.1 Optimization results for CAISO with both reserve and regulation services

7.1.1 Simulation setup

The optimization formulation is applied to a more comprehensive configuration of IES, including LWRS, BoP, HTSE, load, photovoltaic (PV), wind and the electrical grid, considering both regulation and reserve market, like day-ahead market in California Independent System Operator (CAISO).

Electricity and ancillary services (regulation up/down, spinning, and non-spinning) are dispatched hourly, while other decision variables within the IES, such as real power output from PVs and hydrogen production rates, are determined every 5 minutes. The operational horizon (T) for the model is set at 24 hours. Energy, regulation up/down, spinning, and non-spinning reserve prices for the node Summit_6_N001 on May 14th, 2024, in the CAISO market are illustrated in Figure 16. Price trends show peaks typically between 6-8 AM and 7-9 PM, with energy prices generally surpassing those of regulation services, which in turn are higher than both spinning and non-spinning reserves.

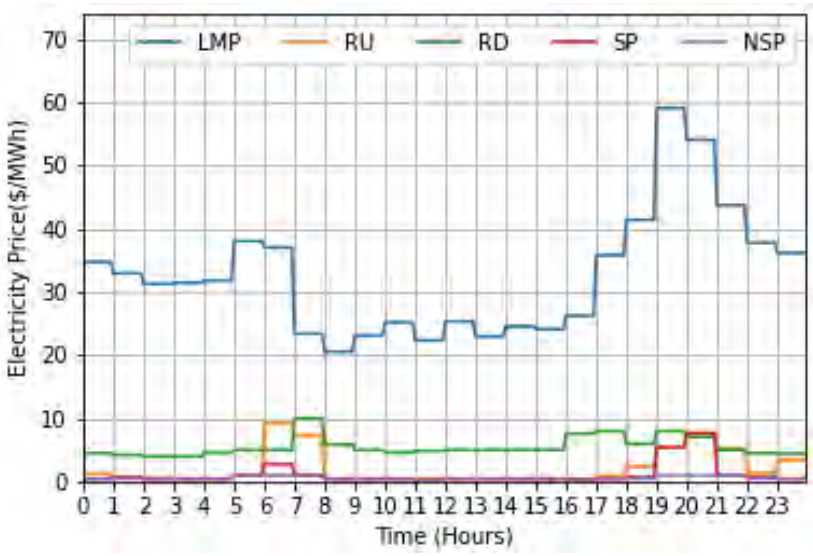

Figure 16 A 24-hour overview of electricity prices for energy (LMP), regulation up (RU), regulation down (RD), spinning (SP), and non-spinning reserve (NSP).

To assess the economic performance of the IES, we assume that IES’s offer is accepted by CAISO. The optimization model, developed in Python using Pyomo and solved with CPLEX, is executed on a laptop equipped with 10 cores and 16GB of RAM.

7.1.2 Optimization Results

Figure 17 illustrates the electricity output from the nuclear generator, wind, and PV; consumption by HTSE; electrical demand; and electricity sold to the grid. The balance of electricity ensures that the sum of the electricity consumption by HTSE, the electricity sold to the grid, electrical load equals to the sum of the electricity output of wind turbine, PV, and nuclear generator.

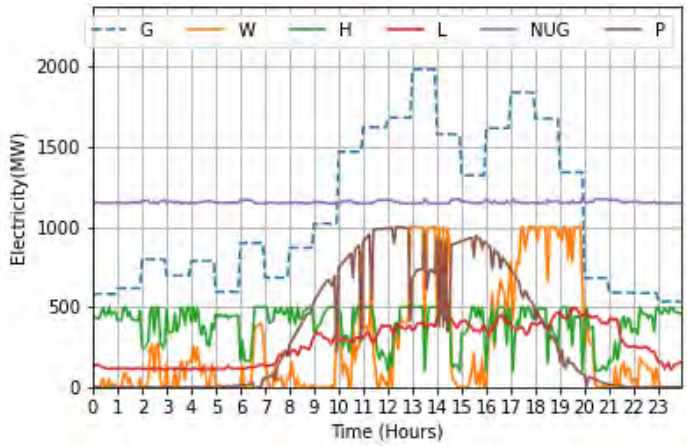

Figure 17 Electricity outputs of the nuclear generator (NUG), wind turbine (W), PV (P), electricity consumption by HTSE (H), electrical load (L), and electricity fed into the electrical grid (G).

Figure 18 displays the dispatch for energy (Energy), regulation-up (RU), regulation-down (RD), spinning reserve (SP), and non-spinning reserve (NSP) over 24 hours. Energy prices are much higher than reserves, so the dispatch of energy is always more than reserves. The electricity revenue is $\$9{,}2 * 10^5$.

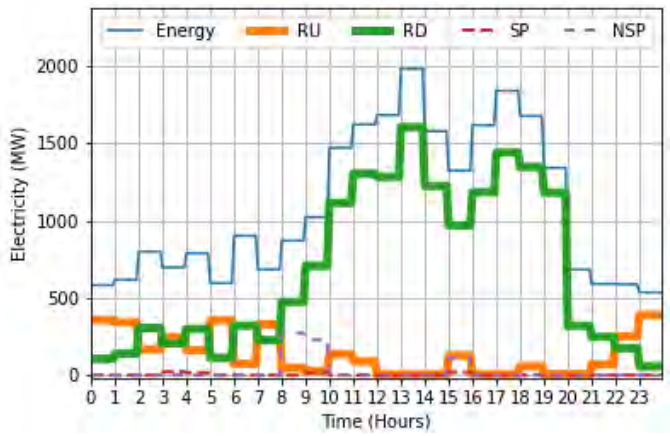

Figure 18 Dispatch for energy (Energy), regulation-up (RU), regulation-down (RD), spinning reserve (SP), and non-spinning reserve (NSP) over 24 hours.

7.2 Results for cases considering low-temperature water electrolysis

7.2.1 Simulation setup

We used the same simulation setup as the scenario for CAISO, which considers both reserve and regulation. However, we replaced HTSE with lower temperature water electrolysis (LTWE).

7.2.2 Optimization results

Figure 19 illustrates the electricity output from the nuclear generator, wind, and PV; consumption by HTSE; electrical demand; and electricity sold to the grid. The balance of electricity ensures that the sum of the electricity consumption by LTWE, the electricity sold to the grid, electrical load equals to the sum of the electricity output of wind turbine, PV, and nuclear generator.

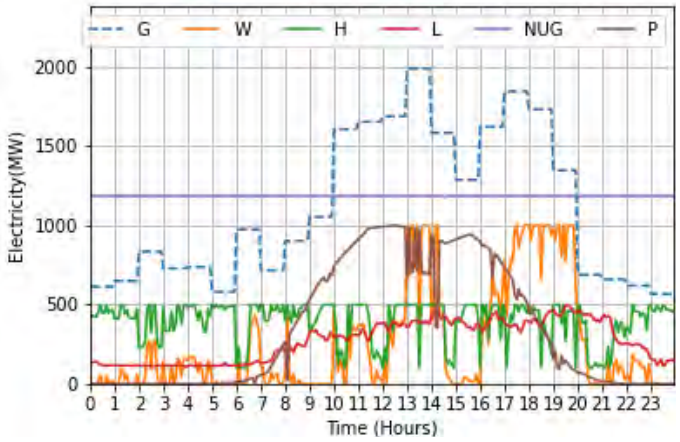

Figure 19. Electricity outputs of the nuclear generator (NUG), wind turbine (W), PV (P), electricity consumption by LTWE (H), electrical load (L), and electricity fed into the electrical grid (G).

Figure 20. displays the dispatch for energy (Energy), regulation-up (RU), regulation-down (RD), spinning reserve (SP), and non-spinning reserve (NSP) over 24 hours. Energy prices are much higher than reserves, so the dispatch of energy is always more than reserves. The electricity revenue is $\$9.45 * 10^5$

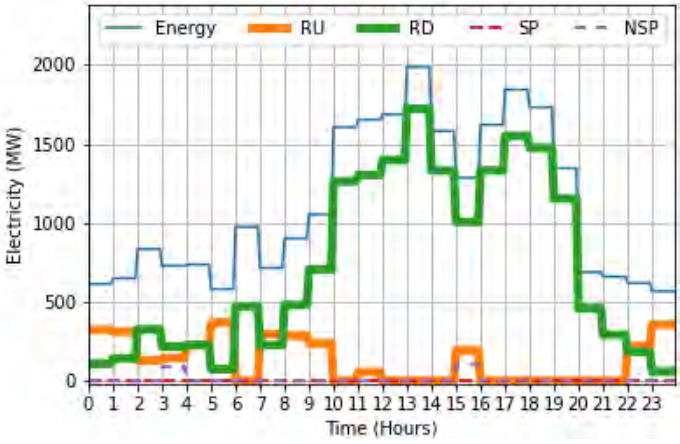

Figure 20. Dispatch for energy (Energy), regulation-up (RU), regulation-down (RD), spinning reserve (SP), and non-spinning reserve (NSP) over 24 hours.